Sparsity-driven super-resolution in clinical contrast-enhanced ultrasound

Ruud J.G. van Sloun[1], Oren Solomon[2], Yonina C. Eldar[2], Hessel Wijkstra[1,3] and Massimo Mischi[1]
[1]Lab. of Biomedical Diagnostics, Eindhoven University of Technology, the Netherlands
[2]Technion - Israel Institute of Technology, Haifa, Israel
[3]Academical Medical Center University Hospital, Amsterdam, the Netherlands

Abstract—**Super-resolution ultrasound enables detailed assessment of the fine vascular network by pinpointing individual microbubbles, using ultrasound contrast agents. The fidelity and achieved resolution of this technique is determined by the density of localized microbubbles and their localization accuracy. To obtain high densities, one can evaluate extremely sparse subsets of microbubbles across thousands of frames by using a very low microbubble dose and imaging for a very long time, which is impractical for clinical routine. While ultrafast imaging somewhat alleviates this problem, long acquisition times are still required to enhance the full vascular bed. As a result, localization accuracy remains hampered by patient motion. Recently, sparsity-based ultrasonic super resolution hemodynamic imaging was proposed, featuring a high spatial as well as temporal resolution by exploiting the temporal correlation structure of flowing microbubbles. However, when using clinical scanners operating at low frame-rates, this pixel-wise correlation across imaging frames may vanish. The aim of this work is hence twofold. First, to attain high microbubble localization accuracy on dense contrast-enhanced ultrasound data using a clinical dose of ultrasound contrast agents and a standard clinical scanner. Second, to retain a high resolution by adequate motion compensation.**

I. INTRODUCTION

SUPER-resolution ultrasound is a recently emerging imaging technology that enables detailed assessment of the fine vascular network by translating concepts from fluorescence photo-activated localization microscopy (FPALM, [1]) to ultrasound. While FPALM localizes active and isolated fluorophores, super-resolution ultrasound exploits ultrasound-contrast-agents: inert gas microbubbles (MBs) that are sized similarly to red blood cells. Hence, they remain intravascular. By pinpointing individual isolated MBs with high precision across many frames, one can circumvent the diffraction limit and reconstruct an image at a 10-fold increase in resolution [2]. The availability of such an imaging technique in clinical practice can open up new possibilities for precise vascular characterization in the context of localizing tumor-driven angiogenesis, or assessment of impaired cardiac perfusion. In this paper, we apply sparse signal recovery techniques to attain super resolution on highly dense, clinically acquired contrast-enhanced ultrasound (CEUS) images.

Typically, extremely sparse subsets of MBs are evaluated across thousands of frames by using a very low MB dose and imaging for a very long time. Such conditions enable isolating individual bubbles effectively; however, in particular imaging for a long time is impractical in clinical routine. While high-frame-rate imaging somewhat alleviates this problem [3], long acquisition times (on the order of minutes) are still required to cover the full vascular bed. Alternatively, and more practically, one can increase the density of MBs to a clinical dose. However, this causes the point-spread-functions of bubbles to overlap severely, invalidating the widely used single-particle localization methods [4].

In optics, a similar trade-off between acquisition time and localization accuracy was addressed by the introduction of super-resolution optical fluctuation imaging (SOFI), which features a moderate resolution gain within short acquisition times [5]. Bar-Zion *et al.* translated the principles of SOFI to CEUS, by relying on the temporal statistics of demodulated echoes of flowing MBs between consecutive frames, demonstrating a moderate spatial resolution gain, but with a temporal resolution of hundreds of milliseconds [6]. More recently, the introduction of sparsity-based ultrasonic super resolution hemodynamic imaging (SUSHI) [7] led to further increase in the spatial resolution, while maintaining sub-second temporal resolution. This ultrasound method exploits sparsity in the temporal correlation structure of fluctuating MBs at a very high frame-rate (e.g. by using plane-wave imaging). However, when scanning with low frame-rates as in most clinical scanners, this distinct correlation is no longer observable in the acquired movie, as the MBs decorrelation time is merely a few milliseconds [3]; much smaller than the temporal resolution. We note that SUSHI could then in principle still be implemented as a frame-by-frame technique, not exploiting temporal MB correlation.

In fluorescence microscopy, several similar strategies have been developed for emitter localization in highly dense scenarios. These methods are either based on fitting clusters of overlapped spots with a fixed number of point-spread-functions (e.g. DAOSTORM [8]), or based on sparse-recovery (e.g. CS-STORM [9] and SPIDER [10]). The latter efficiently enables high-density localization by the combination of inverse image reconstruction with an additional regularization that imposes sparsity of the solution [11].

Here, we apply similar sparse signal recovery techniques to attain super-resolution on highly dense, clinically acquired
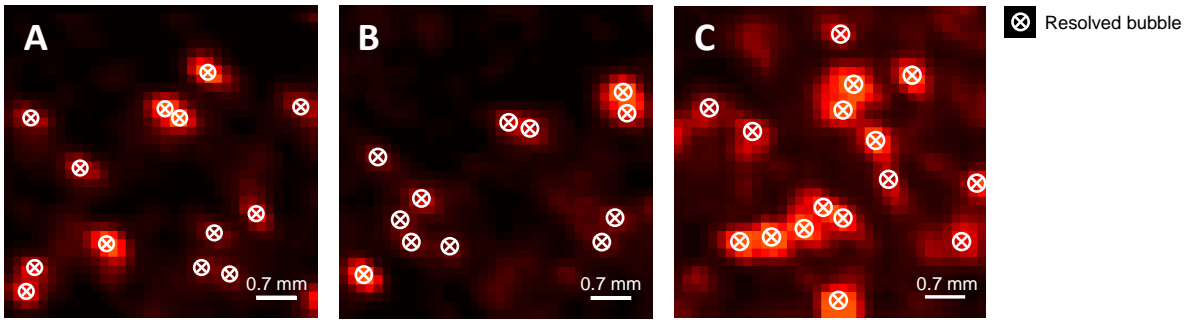
Figure 1: Selected examples of microbubble (MB) location recovery using the proposed algorithm with varying MB densities. (a,b) Localization for relatively low densities, with several overlapping point-spread-functions. (c) Localization for high densities, with many overlapping point-spread-functions.

in-vivo CEUS images of a human prostate. By modeling an individual CEUS frame as the convolution of the MB distributions with the system point spread function (PSF), we employ sparse reconstruction techniques (like a frame-by-frame implementation of SUSHI) to recover the MB positions even in scenarios with extensive overlap. A dedicated registration algorithm is then used to compensate for the inevitable presence of tissue motion and probe drift in this clinical scenario.

The clinical CEUS data acquisition protocol is given in Section II-A, after which the adopted motion compensation and sparse recovery algorithms are presented in Sections II-B and II-C, respectively. The results are described in Section III, and conclusions are drawn in Section IV.

II. METHODS

A. Data acquisition

The *in-vivo* CEUS data was acquired at the AMC University Hospital (Amsterdam, the Netherlands). An intravenous injection of a 2.4-ml MB bolus (SonoVue®, Bracco, Milan, Italy) was administered, and its passage through the prostate was imaged using a C10-3v transrectal endfiring ultrasound probe. The CEUS loops were acquired and stored using a Philips iU22 ultrasound system (Philips Healthcare, Bothell, WA). A dual-screen view was selected to simultaneously obtain fundamental mode as well as contrast-specific imaging data. The axial resolution of the ultrasound system is approximately 0.3 mm and its lateral resolution is on the order of 0.5 mm at 5 cm from the probe. At this distance, the elevational beamwidth is approximately 3.4 mm. The pixel spacing is 0.146 mm in both directions. Imaging was performed for 120 seconds to record the full in- and out-flow of the injected MB bolus. The data was then linearized according to [12] in order to obtain the ultrasound intensities from the log-compressed and quantized image data.

B. Sparse recovery

We model the measured CEUS frames as:

$$\mathbf{y} = \mathbf{Ax}, \tag{1}$$

where $\mathbf{x}$ is a vector which describes the MB distribution on a high-resolution image grid, $\mathbf{y}$ is the vectorized frame of the CEUS loop, and $\mathbf{A}$ is the measurement matrix where each column of $\mathbf{A}$ is the PSF shifted by a single pixel on the high-resolution grid. The PSF of the system is estimated from the data by first manually pinpointing several isolated MB spots from those frames in which only few were present. These spots were then block-windowed and fitted with a rotated anisotropic 2D Gaussian kernel to mitigate the impact of noise on the PSF.

Given the PSF, the goal is now to obtain the MB vector $\mathbf{x}$ from the measurements $\mathbf{y}$ according to (1). With $\mathbf{x}$ defined on a much denser grid than the original CEUS frame, this is an ill-posed problem, requiring the use of some form of regularization. If we assume that the MB distribution is sparse on a sufficiently high-resolution grid, i.e. $||\mathbf{x}||_0$ (number of non-zero entries in $\mathbf{x}$) is low, then we can formulate the following regularized problem:

$$\hat{\mathbf{x}} = \underset{\mathbf{x}}{\text{argmin}} \quad ||\mathbf{y} - \mathbf{Ax}||_2^2 + \lambda||\mathbf{x}||_0$$
$$\text{subject to} \quad \mathbf{x} \geq 0, \tag{2}$$

where λ is a parameter that determines the influence of the sparsity-promoting penalty $||\mathbf{x}||_0$ on the estimate. The problem described in (2) is however an NP-hard combinatorial problem. To make the solution tractable, we resort to a widely adopted heuristic alternative to (2), by replacing $||\mathbf{x}||_0$ with $||\mathbf{x}||_1$ [13]:

$$\hat{\mathbf{x}} = \underset{\mathbf{x}}{\text{argmin}} \quad ||\mathbf{y} - \mathbf{Ax}||_2^2 + \lambda||\mathbf{x}||_1$$
$$\text{subject to} \quad \mathbf{x} \geq 0. \tag{3}$$

To facilitate high-resolution MB localization, the grid on which $\mathbf{x}$ is assessed is oversampled by a factor of 4 with respect to the original pixel grid. We divided the up-sampled CEUS frames into partially overlapping patches of size 128×128, which were processed separately. The results for all these subregions are then stitched together.

For each region, (3) is numerically solved using the Fast Iterative Shrinkage Thresholding Algorithm (FISTA), a fast proximal gradient method [14]. The FISTA algorithm is modified to only consider non-negative values for $\mathbf{x}$. After estimating $\mathbf{x}$ for each frame, the estimated MB distributions
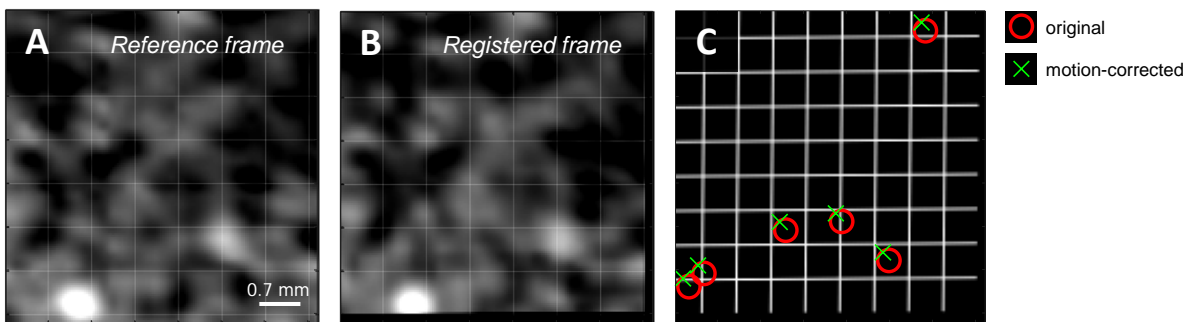
Figure 2: (a) First up-sampled fundamental mode image in the sequence, serving as the reference frame. (b) Resulting registration of a frame captured 3 seconds later. (c) Motion-corrected microbubble locations.

in $\mathbf{x}$ are summed across all frames to yield the final super-resolution image.

C. Motion compensation

To correct the detected high-resolution MB distribution for tissue motion, we first extract the pure-tissue signal from the fundamental mode images. With the aim of separating those components originating from tissue, MBs, and noise, we formulate the source extraction problem as a subspace selection problem. To this end, we perform a singular value decomposition (SVD) on the full space-time CEUS data (*i.e.* a matrix of which the columns are the vectorized frames), and attribute the first k singular values to tissue. The resulting rank-k approximation of the original space-time matrix that is based on these low-order singular values yields signal components with high spatiotemporal coherence. Such an approach was recently introduced as a highly effective clutter filtering strategy to remove tissue signal [15]. Here we exploit it for tissue-signal extraction rather than removal. For each subregion/patch, we determine the affine transformation that maps the image data back to the first frame in the loop, by minimizing the mean squared error among those patches. We use MATLAB's (The MathWorks, Natick, MA) `imregtform` function for this purpose. We then apply the same transformation to the estimated MB distribution $\hat{\mathbf{x}}$ to adequately compensate for displacements induced by tissue motion. While this patch-based approach effectively deals with probe-motion (translation) and to some extent local strain (scaling), it is limited to in-plane transformations. Motion compensation is performed after MB localization to avoid distortion of the system PSF following the affine transformation.

III. RESULTS

Several examples of MB localization based on sparse recovery are given in Figure 1. Compared to (a,b), the detected MB density is notably higher in (c), demonstrating the method's ability to deal with varying densities and signal intensities.

In Figure 2, we exemplify the adopted motion compensation procedure and indicate how this impacts the MB location estimates.

Figure 3 shows the obtained super-resolution ultrasound image of a region of interest in the human prostate. In total,

300 frames were used to construct this image, which were taken during the wash-out phase of the CEUS acquisition. The proposed sparse-recovery method reveals fine details that are not visible in the diffraction limited maximum-intensity projection.

IV. CONCLUSIONS AND DISCUSSION

In this paper, a new super-resolution ultrasound method that is designed specifically to deal with high-density clinically-acquired CEUS data is presented. By adapting sparse reconstruction techniques as used in fast super-resolution fluorescence microscopy and SUSHI, and combining them with effective motion compensation, the proposed method enables high resolution imaging of the perfused vasculature in a standard clinical setting.

We observed that bubbles can be localized (Figure 1), even if their PSFs show significant overlap. Moreover, the method yields plausible position estimates for varying densities, without adapting the algorithm parameters (e.g. the sparsity-promoting penalty λ).

A qualitative exemplification of the results obtained with this principle is shown in Figure 3, where complex and fine vascular structures are revealed. This level of detail was achieved with merely 300 image frames, which was predominantly limited by the increasingly impaired robustness of motion compensation after longer accumulation times.

Tissue motion impedes the achievable resolution and fidelity of super-resolution methods. Although dedicated registration techniques were exploited to mitigate its impact, one can not account for out-of-plane movements which are in practice inevitable. This stresses the need for methods that can reach a high density of localized bubbles in a very short time in a clinical setting, and exploitation of 3D ultrasound acquisitions that facilitate complete registration in all directions.

The initial results presented in this work are promising and yield plausible outcomes. Yet, a more extensive study is required to validate the proposed approach. The localization performance should be thoroughly assessed *in-silico* and, ideally, to some extent *in-vitro*. The latter poses challenges on its own, as microfabrication of vascular structures is in practice not an easy task. These aspects, along with optimization of the
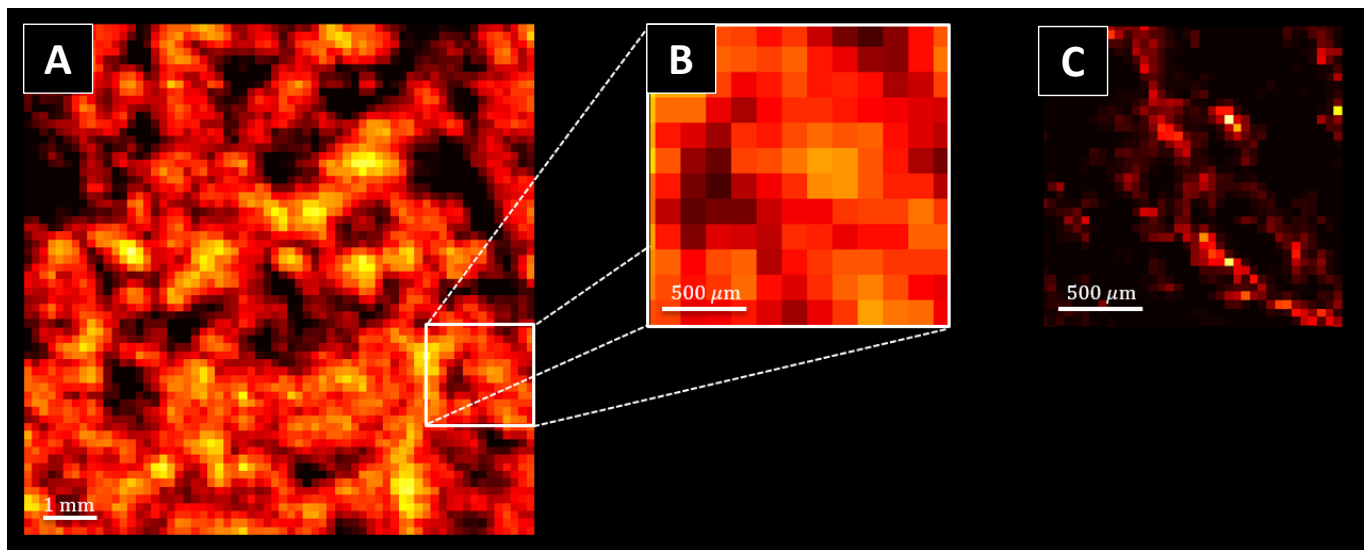
Figure 3: (a) Standard maximum intensity projection of a CEUS acquisition in a human prostate and (b) a selected area in the image. (c) Sparsity-driven super-resolution ultrasound on the same area.

adopted algorithm and exhaustive comparison with alternative super-resolution methods, are therefore part of future work.

REFERENCES

[1] Eric Betzig, George H Patterson, Rachid Sougrat, O Wolf Lindwasser, Scott Olenych, Juan S Bonifacino, Michael W Davidson, Jennifer Lippincott-Schwartz, and Harald F Hess. Imaging intracellular fluorescent proteins at nanometer resolution. *Science*, 313(5793):1642–1645, 2006.

[2] Yann Desailly, Olivier Couture, Mathias Fink, and Mickael Tanter. Sono-activated ultrasound localization microscopy. *Applied Physics Letters*, 103(17):174107, 2013.

[3] Claudia Errico, Juliette Pierre, Sophie Pezet, Yann Desailly, Zsolt Lenkei, Olivier Couture, and Mickael Tanter. Ultrafast ultrasound localization microscopy for deep super-resolution vascular imaging. *Nature*, 527(7579):499–502, 2015.

[4] Michael J Rust, Mark Bates, and Xiaowei Zhuang. Sub-diffraction-limit imaging by stochastic optical reconstruction microscopy (storm). *Nature methods*, 3(10):793–796, 2006.

[5] Thomas Dertinger, Ryan Colyer, Gopal Iyer, Shimon Weiss, and Jörg Enderlein. Fast, background-free, 3d super-resolution optical fluctuation imaging (sofi). *Proceedings of the National Academy of Sciences*, 106(52):22287–22292, 2009.

[6] Avinoam Bar-Zion, Charles Tremblay-Darveau, Oren Solomon, Dan Adam, and Yonina C Eldar. Fast vascular ultrasound imaging with enhanced spatial resolution and background rejection. *IEEE transactions on medical imaging*, 36(1):169–180, 2017.

[7] Avinoam Bar-Zion, Oren Solomon, Charles Tremblay-Darveau, Dan Adam, and Yonina C Eldar. Sparsity-based ultrasound super-resolution imaging. In *Proceedings of the 23rd European symposium on Ultrasound Contrast Imaging*, pages 156–157. ICUS, 2017.

[8] Seamus J Holden, Stephan Uphoff, and Achillefs N Kapanidis. Daostorm: an algorithm for high-density super-resolution microscopy. *Nature methods*, 8(4):279–280, 2011.

[9] Lei Zhu, Wei Zhang, Daniel Elnatan, and Bo Huang. Faster storm using compressed sensing. *Nature methods*, 9(7):721–723, 2012.

[10] Siewert Hugelier, Johan J De Rooi, Romain Bernex, Sam Duwé, Olivier Devos, Michel Sliwa, Peter Dedecker, Paul HC Eilers, and Cyril Ruckebusch. Sparse deconvolution of high-density super-resolution images. *Scientific reports*, 6:21413, 2016.

[11] Hazen P Babcock, Jeffrey R Moffitt, Yunlong Cao, and Xiaowei Zhuang. Fast compressed sensing analysis for super-resolution imaging using l1-homotopy. *Optics express*, 21(23):28583–28596, 2013.

[12] MPJ Kuenen, M Mischi, and H Wijkstra. Contrast-ultrasound diffusion imaging for localization of prostate cancer. *IEEE Transactions on Medical Imaging*, 30(8):1493–1502, 2011.

[13] Yonina C Eldar and Gitta Kutyniok. *Compressed sensing: theory and applications*. Cambridge University Press, 2012.

[14] Amir Beck and Marc Teboulle. A fast iterative shrinkage-thresholding algorithm for linear inverse problems. *SIAM journal on imaging sciences*, 2(1):183–202, 2009.

[15] Charlie Demené, Thomas Deffieux, Mathieu Pernot, Bruno-Félix Osmanski, Valérie Biran, Jean-Luc Gennisson, Lim-Anna Sieu, Antoine Bergel, Stéphanie Franqui, Jean-Michel Correas, et al. Spatiotemporal clutter filtering of ultrafast ultrasound data highly increases doppler and fultrasound sensitivity. *IEEE transactions on medical imaging*, 34(11):2271–2285, 2015.